Window Function Design for Non-uniform MIMO Array

1st Mingsai Huan
School of Electronics and Information
Northwestern Polytechnical University
Xi'an, China
huanmingsai@163.com

2nd Baoxi Guo
School of Electronics and Information
Northwestern Polytechnical University
Xi'an, China
2015301863@mail.nwpu.edu.cn

3rd Yu Tu
School of Electronics and Information
Northwestern Polytechnical University
Xi'an, China
yutu@mail.nwpu.edu.cn

4th Junli Liang
School of Electronics and Information
Northwestern Polytechnical University
Xi'an, China
liangjunli@nwpu.edu.cn

5th Yugang Ma
Institute for Infocomm Research (I2R)
*A*STAR*
Singapore
mayg@i2r.a-star.edu.sg

6th Yonghong Zeng
Institute for Infocomm Research (I2R)
*A*STAR*
Singapore
yhzeng@i2r.a-star.edu.sg

***Abstract*—Antenna position errors caused by manufacturing accuracy limits lead to a great difference between the real and ideal models of antenna arrays in extremely high frequency (EHF) band MIMO radar with tiny physical elements and pitches. As the real array is actually a non-uniform array, the conventional window function fails when applied to non-uniform sampling data, which causes angular ambiguities and seriously degrades the performance of DOA estimation. Based on an advanced analysis of spectral distortion in non-uniform sampling, this paper introduces a novel method to design a specialized window function for non-uniform MIMO arrays, aiming to minimize the equivalent noise bandwidth (ENBW) while sufficiently suppress the sidelobe level (SLL). The simulation results show the effectiveness of the proposed window function, which reduces angular ambiguities and thereby improves the performance of DOA estimation in practical applications.**

***Index Terms*—Non-uniform Sampling, Non-uniform Array, Window Function, DOA estimation, MIMO Radar**

I. Introduction

Multiple-input multiple-output (MIMO) millimeter-wave radar [1] has been widely used in different applications such as autonomous driving [2] and assisted living [3], due to its capability to achieve high angular resolution with a small number of antennas. Since the wavelength of millimeter wave or terahertz radar is very short, the existing low manufacturing accuracy may lead to a large antenna position deviation compared to the wavelength. Therefore, the great difference between the ideal model and real model of antenna arrays should be taken into account in practice.

This work was supported by the China Scholarship Council (CSC) under Grant Liu Jin Xuan [2022] No. 87, the Key Research and Development Program of Shaanxi under Grant 2021SF-166, Innovation Foundation for Doctor Dissertation of Northwestern Polytechnical University, Aeronautical Science Foundation of China under Grant 201920053001. This research is supported by the National Research Foundation, Singapore and Infocomm Media Development Authority under its Future Communications Research & Development Programme (Grant award number: FCP-ASTAR-TG-2022-003). (Corresponding author: Junli Liang.)

The non-idealities of antenna arrays are often ignored in conventional direction of arrival (DOA) estimation methods. If the ideal model is used directly for DOA estimation in real arrays, the performance will degrade or even fail. For example, Cox et al. [4] discussed the impact of steering vector mismatch on Capon beamforming, and [5] evaluated the influence of model errors on multiple signal classification (MUSIC) performance. Therefore, in practical applications, it is necessary to calibrate the position errors of array elements before use [6].

Moreover, it is worth noting that the real array, i.e., the calibrated array, is actually a random non-uniform array. Although the calibration has been performed, using conventional DOA estimation directly for non-uniform arrays presents many drawbacks. However, most existing works do not pay attention to this problem. [7] analyzes the relationship between the geometry of non-uniform MIMO arrays and angular ambiguities, which shows that angular ambiguities often occur in non-uniform arrays. Therefore, new methods are needed to compensate the performance degradation caused by non-uniform arrays.

As DOA estimation is closely related to spectrum estimation, a feasible approach is to utilize windowing techniques [8] to preprocess data which attenuates spectral leakage. However most window functions are designed for uniform sampling, while they fail in non-uniform sampling. In recent years, some window function design methods have been proposed to improve the performance of special MIMO arrays. A window function is designed for compact MIMO arrays in [9], which forms a narrower main beam compared to conventional beamforming methods, but it also cannot be used in non-uniform arrays. In [10], a new model is proposed for jointly optimizing the position of array elements and the window function. Since this model is non-convex, usually only a suboptimal solution can be found via the simulated annealing algorithm.

In this paper, we introduce a non-uniform sampling window

function and analyze the spectral distortion of windowed non-uniform sampling signals in detail. Then, the window function design for non-uniform arrays is formulated as a convex problem which is easy to solve. The simulation outcomes demonstrate the effectiveness of the proposed window function, which reduces angular ambiguities in the real MIMO array, leading to enhanced DOA estimation performance in practical applications.

II. Window Function Design for Non-uniform MIMO Array

A. MIMO Array

Consider a collocated MIMO radar system with M transmitting antennas and N receiving antennas, the vectors $\boldsymbol{t} = [t_1, \ldots, t_M]^{\mathsf{T}}$ and $\boldsymbol{r} = [r_1, \ldots, r_N]^{\mathsf{T}}$ are the positions of transmitting and receiving antennas respectively, which are normalized by wavelength λ of propagation. Then the far-field narrow-band transmitting and receiving steering vectors toward θ are given by:

$$\boldsymbol{a}_t(\theta) = e^{-j2\pi \boldsymbol{t} \sin\theta}, \tag{1}$$

$$\boldsymbol{a}_r(\theta) = e^{-j2\pi \boldsymbol{r} \sin\theta}. \tag{2}$$

where $\theta \in [-\pi/2, \pi/2]$ is the angle between the target and bore-sight direction. The virtual aperture of a MIMO system can be constructed through transmitting M orthogonal waveforms and filtering the receive signals by M matched-filters, which generate $M \times N$ virtual channels. The $M \times N$ positions of generated virtual elements are given by $\boldsymbol{v} = [t_1+r_1, t_1+r_2, \ldots, t_1+r_N, t_2+r_1, \ldots, t_2+r_N, \ldots, t_M+t_N]^{\mathsf{T}}$. The steering vector of the virtual array is expressed as a Kronecker product form:

$$\boldsymbol{a}(\theta) = \boldsymbol{a}_t(\theta) \otimes \boldsymbol{a}_r(\theta) = e^{-j2\pi \boldsymbol{v} \sin\theta}. \tag{3}$$

B. Spectral Distortion of Non-uniform Sampling

Typically, the virtual array of MIMO radar is a uniform array with half-wavelength element spacing. However, antenna position errors caused by low manufacturing accuracy and mutual coupling lead to a great difference between the ideal and real models of antenna arrays in practice. Because the real MIMO array is no longer uniform, it is necessary to investigate the DOA estimation performance of non-uniform arrays.

Assume that a virtual element at the position x receives a plane wave signal from direction θ, which is described by

$$a(\theta) = e^{-j2\pi x \sin(\theta)}. \tag{4}$$

Define a spatial frequency variable $u = \sin(\theta)$, whose unit is Hz, then the spatial domain signal can be written in u frequency domain form

$$a(u) = e^{-j2\pi x u}. \tag{5}$$

This means that the DOA estimation problem is essentially a spectrum estimation problem, and there is a Fourier transform relationship between x and u. The sampling of spatial signals by a finite-length non-uniform array can be regarded as non-uniform sampling and windowing in the spatial domain. To express this non-uniform sampling process, we define the sampling function (or aperture function) as

$$s(x) = \sum_{l=1}^{L} \delta(x - x_l), \tag{6}$$

where x_l is the spatial sampling position, L is the number of sampling points, and $\delta(x)$ is a unit impulse signal

$$\delta(x) = \begin{cases} 1, & x = 0 \\ 0, & x \neq 0 \end{cases} \tag{7}$$

The non-uniform sampling process for a spatial analog signal $p_a(x)$ can be considered as its multiplication by the sampling function $s(x)$, i.e.

$$p(x) = p_a(x) \cdot s(x) = p_a(x) \cdot \sum_{l=1}^{L} \delta(x - x_l). \tag{8}$$

According to the properties of Fourier transform, the multiplication in time domain is equivalent to a convolution in frequency domain. Perform a Fourier transform on both sides of (8), then the spatial spectrum $P(u)$ can be written as

$$P(u) = P_a(u) * S(u) = \int_{-\infty}^{\infty} P_a(\tau) \cdot S(u - \tau)\, \mathrm{d}\tau, \tag{9}$$

where

$$S(u) = \int_{-\infty}^{\infty} s(x) \cdot e^{-\mathrm{j}2\pi x u}\, \mathrm{d}x = \sum_{l=1}^{L} \exp(-\mathrm{j}2\pi x_l u), \tag{10}$$

and $P_a(u)$ is the Fourier transform of $p_a(x)$. Here we give two examples, with a sampling length (aperture size) of $X = 7.5(\lambda)$, the uniform and non-uniform sampling functions and their spectra are drawn in Fig. 1.

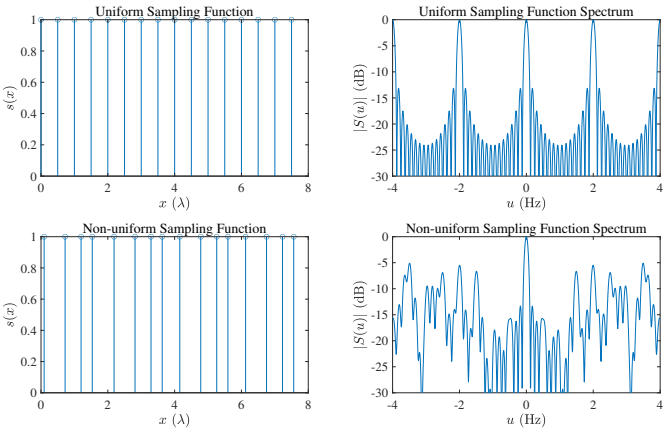


Fig. 1. Sampling functions and their spectra.

Uniform sampling: In the upper graphs of Fig. 1, the sampling rate is set to $U_s = 2$Hz, corresponding to a half-wavelength element spacing. According to the theory of discrete Fourier transform, the period of the spectrum is equal to the sampling rate. The Nyquist–Shannon sampling theorem demonstrates that spectral aliasing does not occur when the

bandwidth of $p_a(x)$ satisfies $B < U_s$. For a spatial signal, there must be $B \leq 2$Hz, because $u = \sin(\theta) \in [-1, 1]$.

Since the sampling function is also a rectangular window function, spectral leakage occurs, and the spectrum shows a shape of periodic sinc function, with a sidelobe level (SLL) of -13.26 dB. The main lobe width (MLW) of the spectrum determines the spatial frequency resolution and also angular resolution of the sampled signal, while the high side lobes of spectrum leakage may cause mutual interference between signals of different spatial frequencies, i.e., different directions. In practice, the SLL can be reduced by data windowing, but the main lobe width will increase consequently, that is, the frequency resolution is usually sacrificed because of windowing, and thus there is a trade-off between the SLL and MLW. For example, the upper graphs in Fig. 2 show the uniform sampling function and spectrum using the Chebyshev window [11], with a equal SLL of -20dB.

Non-uniform sampling: According to the real positions of MIMO virtual elements from a 77GHz 4T4R mmWave radar sensor (see Fig. 4), a small shift is imposed on the uniform sampling positions, as shown in the lower graphs of Fig. 1. Unlike the spectrum of uniform sampling function, the non-uniform one is not periodic [12]. Due to the combined effects of window function and non-uniform sampling, higher non-periodic side lobes appear in the spectrum. Because we can not distinguish which is the aliasing caused by non-uniform sampling and which is the leakage caused by window function, these effects are referred to as the spectral distortion of non-uniform sampling in this paper. The bottom of Fig. 2 indicates that adding a Chebyshev window to non-uniformly sampled data does not attenuate the spectral distortion, which is due to the fact that the existing window functions are designed for uniform sampling. The high SLL in the spectrum of non-uniform sampling leads to angular ambiguities in the DOA estimation. Therefore, the special window function is designed for non-uniform arrays in this study, in order to avoid angular ambiguities.

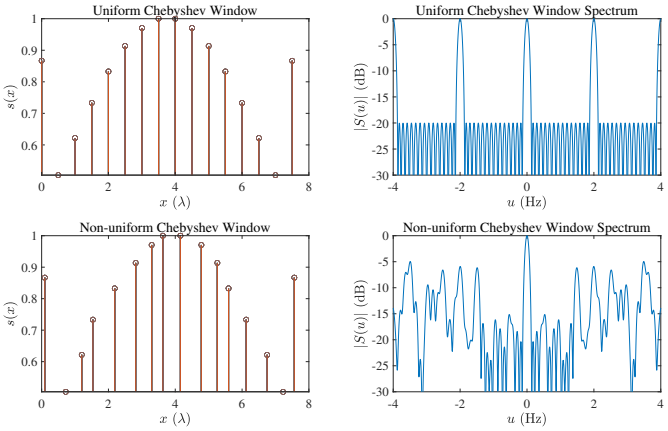


Fig. 2. Chebyshev sampling functions and their spectra.

C. Non-uniform Window Function Design

Define window coefficients as $\boldsymbol{w} = [w_1, \ldots, w_L]^{\mathsf{T}}$, the non-uniform window function can be written as

$$s(\boldsymbol{w}, x) = \sum_{l=1}^{L} w_l \delta(x - x_l), \tag{11}$$

and its spectrum is given by

$$S(\boldsymbol{w}, u) = \int_{-\infty}^{\infty} s(\boldsymbol{w}, x) \cdot e^{-\mathrm{j}2\pi x u} \, \mathrm{d}x = \sum_{l=1}^{L} w_l \exp(-\mathrm{j}2\pi x_l u). \tag{12}$$

Then the spectrum of windowed sampled signal becomes

$$P(u) = P_a(u) * S(\boldsymbol{w}, u) = \int_{-\infty}^{\infty} P_a(\tau) \cdot S(\boldsymbol{w}, u - \tau) \, \mathrm{d}\tau, \tag{13}$$

According to the properties of convolution, as $S(\boldsymbol{w}, u)$ gets closer to the impulse signal, the sampled signal spectrum $P(u)$ gets closer to the spatial analog signal spectrum $P_a(u)$. Obviously, it is impossible to approximate the impulse signal over the entire spectrum. For an analog signal with a bandwidth of B, the spectral distortion outside the bandwidth can be ignored after filtering. As long as $S(\boldsymbol{w}, u)$ approximates the impulse signal in the $u \in [-B, B]$ interval, with a narrow MLW and a low SLL, the spectral distortion caused by non-uniform sampling can be attenuated. Specifically, the SLL of $S(\boldsymbol{w}, u)$ in the interval $u \in [-B, B]$ determines the degree of spectral distortion, while the MLW determines spatial frequency resolution.

In general, the window coefficients $\boldsymbol{w}$ should be real and nonnegative to ensure a symmetric spectrum and avoid phase inversion [8]. This symmetry allows us to consider only half of the interval, i.e., $u \in [0, B]$. Define a main lobe to side lobe transition point as u_b, then the side lobe region can be discretized to Q grids given by

$$u_q = u_b + \frac{q-1}{Q-1}(B - u_b), \; q = 1, \ldots, Q. \tag{14}$$

The peak value of the main lobe is

$$\max_u S(\boldsymbol{w}, u) = S(\boldsymbol{w}, 0) = \sum_{l=1}^{L} w_l = \mathbf{1}^{\mathsf{T}} \boldsymbol{w}. \tag{15}$$

If the desired peak-to-side-lobe ratio (PSLR) is ϵ, the PSLR constraints can be written as

$$\frac{S(\boldsymbol{w}, u_q)}{\mathbf{1}^{\mathsf{T}} \boldsymbol{w}} \leq \epsilon, \quad q = 1, \ldots, Q. \tag{16}$$

Since (12) is an expression of a non-uniform discrete Fourier transform (NUDFT), (16) can be further written in a matrix form

$$\frac{\boldsymbol{F}\boldsymbol{w}}{\mathbf{1}^{\mathsf{T}} \boldsymbol{w}} \preceq \epsilon \cdot \mathbf{1} \tag{17}$$

where $\boldsymbol{F}$ is a NUDFT matrix corresponding to the sampling positions $x_1, \ldots, x_L$ and frequencies $u_1, \ldots, u_Q$.

Moreover, the equivalent noise bandwidth (ENBW) [8], which measures the noise performance of the window function, is a very important figure of merit for windown function design, defined by

$$ENBW(\boldsymbol{w}) = \frac{\|\boldsymbol{w}\|^2}{(\mathbf{1}^\mathsf{T}\boldsymbol{w})^2}. \tag{18}$$

The smaller the value of ENBW, the better the performance of the window, in the presence of broadband noise. Therefore, the optimization model is built as

$$\begin{aligned} \min_{\boldsymbol{w}} \quad & \frac{\|\boldsymbol{w}\|^2}{(\mathbf{1}^\mathsf{T}\boldsymbol{w})^2} \\ \text{s.t.} \quad & \frac{\boldsymbol{F}\boldsymbol{w}}{\mathbf{1}^\mathsf{T}\boldsymbol{w}} \preceq \epsilon \cdot \mathbf{1}, \\ & \mathbf{1}^\mathsf{T}\boldsymbol{w} = 1, \\ & \boldsymbol{w} \succeq \mathbf{0}, \end{aligned} \tag{19}$$

where the equality constraint $\mathbf{1}^\mathsf{T}\boldsymbol{w} = 1$ makes the normalized coherence gain of the window function be unity, the same as that of the rectangular window [8], and also ensures that (19) has a unique solution. Then (19) is rewritten as

$$\begin{aligned} \min_{\boldsymbol{w}} \quad & \|\boldsymbol{w}\|^2 \\ \text{s.t.} \quad & \boldsymbol{F}\boldsymbol{w} \preceq \epsilon \cdot \mathbf{1}, \\ & \mathbf{1}^\mathsf{T}\boldsymbol{w} = 1, \\ & \boldsymbol{w} \succeq \mathbf{0}. \end{aligned} \tag{20}$$

It is easy to see that (20) is a quadratic programming (QP) problem, which is convex and can be efficiently solved by using CVX toolbox [13].

III. Simulations

The proposed method is implemented for a 77GHz mmWave MIMO radar evaluation board with four transmitters and four receivers (4T4R). The placement of antenna arrays is shown in Fig. 4. The real transmiiter and receiver positions are $0, 2.0935, 4.0606, 6.0299$ and $0, 0.6274, 1.1057, 1.4408$, respectively, which are obtained by a calibration [6], while the ideal positions are $0, 2, 4, 6$ and $0, 0.5, 1, 1.5$. In the 77GHz millimeter wave band, the manufacturing process of the antenna has caused an error in the array element position up to 0.1274λ.

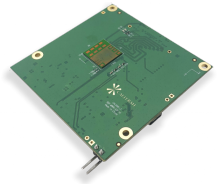


Fig. 3. The 77GHz mmWave radar evaluation board.

In this experiment, we assume that the field-of-view (FoV) of array is set to $\theta \in [\theta_{\min}, \theta_{\max}]$. This means that the bandwidth of spatial signals is limited to

$$B = \sin(\theta_{\max}) - \sin(\theta_{\min}). \tag{21}$$

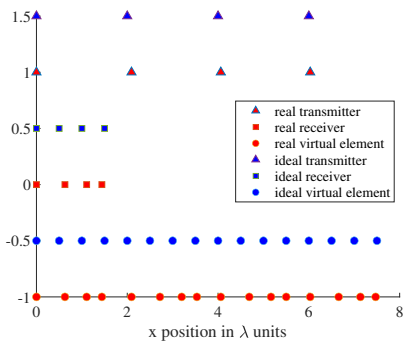
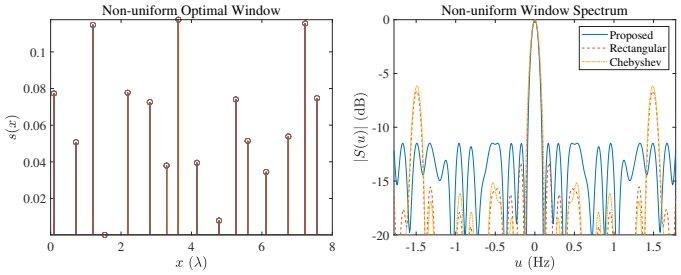


Fig. 4. The placement of ideal array and real array.

In (20), ϵ is set to -11.5dB. Fig. 5(a) gives the optimized window function for the non-uniform MIMO array, with a FoV of $\theta \in [-60°, 60°]$, i.e., a bandwidth of $B = 1.73$Hz. The spectrum of the proposed window is depicted in Fig. 5(b), and compared with that of rectangular window and Chebyshev window. We can see that the SLL of the proposed one is -11.5dB over $u \in [-1.73, 1.73]$, while high side lobes occur in the spectrum of rectangular window (-6.6dB) and Chebyshev window (-6.1dB). The ENBW of the proposed one, rectangular window, and Chebyshev window is 0.081, 0.065, and 0.063, respectively.

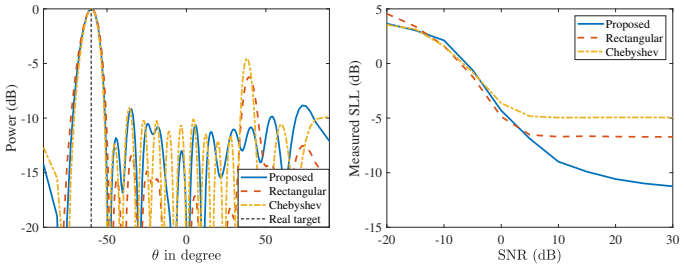


(a) Optimized window function (b) Spectrum

Fig. 5. The optimized window function and its spectrum compared with rectangular window and Chebyshev window.

To investigate the effect of windowing on DOA estimation performance, Fig. 6 shows the results of single-target DOA estimation using non-uniform fast Fourier transform (NUFFT) [14] for the non-uniform array, with different window functions applied to the non-uniform sampling data. Fig. 6(a) gives an example of the estimated spatial spectrum with the target at $-60°$ and an SNR of 10dB. The measured SLL is evaluated as a function of the SNR in Fig. 6(b) (the number of Monte Carlo trials is 500), which demonstrates that the proposed window exhibits a lower SLL especially when the SNR is higher than 5dB.

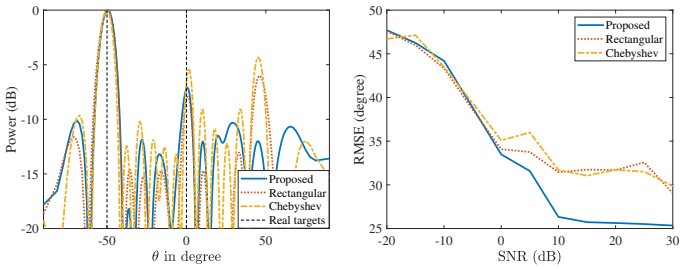
Moreover, a two-target scenario is also considered in Fig. 7. To reflect the impact of strong targets on weak targets, the amplitude ratio of the echoes from two targets is set to 5:1, and their directions are random. An example of estimated spatial spectrum with an SNR of 10dB is depicted in Fig.



(a) An example of spatial spectrum (b) SLL vs SNR

Fig. 6. Single-target DOA estimation using NUFFT with different window functions applied to the non-uniform sampling data.

7(a), and the angular root mean square errors (RMSE) are evaluated as a function of the SNR in Fig. 7(b). As shown in Fig. 7(a), the peak of the weak target is often submerged by sidelobes, making peak detection more prone to mistaking high sidelobes for targets, leading to angular ambiguities or false targets. When the SNR is higher than 0dB, the RMSE of proposed window are lower than that of rectangular window and Chebyshev window, which indicates that the window function designed for non-uniform arrays presented in this paper can significantly reduce angular ambiguities, thereby improve the performance of DOA estimation in practice.



(a) An example of spatial spectrum (b) RMSE vs SNR

Fig. 7. Two-target DOA estimation using NUFFT with different window functions applied to the non-uniform sampling data. The amplitude ratio of the echoes from two targets is 5:1.

IV. Conclusions

The angular ambiguity caused by non-uniform MIMO arrays is an essential problem in practical applications. This paper discussed the spectral distortion caused by windowed non-uniform sampling, which allowed for the analysis of the DOA estimation performance of the non-uniform MIMO array. Then a window function design method suitable for non-uniform arrays was proposed, aiming to minimize the ENBW and sufficiently suppress the SLL. Simulations demonstrate that the proposed window function can effectively reduce angular ambiguities, and hence improve DOA estimation performance of real MIMO arrays.

References

[1] J. Li and P. Stoica, *MIMO Radar Signal Processing*. Hoboken, NJ, USA: John Wiley & Sons, Inc., Oct. 2008.

[2] S. Sun, A. P. Petropulu, and H. V. Poor, "MIMO radar for advanced driver-assistance systems and autonomous driving: Advantages and challenges," *IEEE Signal Process. Mag.*, vol. 37, no. 4, pp. 98–117, 2020.

[3] J. Le Kernec, F. Fioranelli, C. Ding, H. Zhao, L. Sun, H. Hong, J. Lorandel, and O. Romain, "Radar signal processing for sensing in assisted living: The challenges associated with real-time implementation of emerging algorithms," *IEEE Signal Process. Mag.*, vol. 36, no. 4, pp. 29–41, 2019.

[4] H. Cox, "Resolving power and sensitivity to mismatch of optimum array processors," *J. Acoust. Soc. Am.*, vol. 54, no. 3, pp. 771–785, Sep. 1973.

[5] A. Swindlehurst and T. Kailath, "A performance analysis of subspace-based methods in the presence of model errors. I. the MUSIC algorithm," *IEEE Trans. Signal Process.*, vol. 40, no. 7, pp. 1758–1774, Jul. 1992.

[6] C. Vasanelli, F. Roos, A. Durr, J. Schlichenmaier, P. Hugler, B. Meinecke, M. Steiner, and C. Waldschmidt, "Calibration and direction-of-arrival estimation of millimeter-wave radars: A practical introduction," *IEEE Antennas Propag. Mag.*, vol. 62, no. 6, pp. 34–45, 2020.

[7] M. Huan, J. Liang, Y. Wu, Y. Li, and W. Liu, "SASA: super-resolution and ambiguity-free sparse array geometry optimization with aperture size constraints for MIMO radar," *IEEE Trans. Antennas Propag.*, vol. 71, no. 6, pp. 4941–4954, Jun. 2023.

[8] K. M. M. Prabhu, *Window Functions and Their Applications in Signal Processing*. Taylor & Francis, 2014.

[9] Y. Jiang, W. Zhang, H. Li, and C. Luo, "Virtual transmitting-receiving beamforming approach to achieving narrower mainlobe for MIMO radar by tapering," *Proc. Second Int. Conf. Commun. Signal Process. Syst.*, pp. 525–532, 2014.

[10] D. Mateos-Nunez, M. A. Gonzalez-Huici, R. Simoni, F. B. Khalid, M. Eschbaumer, and A. Roger, "Sparse array design for automotive MIMO radar," *EuRAD 2019 - 2019 16th Eur. Radar Conf.*, pp. 249–252, 2019.

[11] F. J. Harris, *Multirate Signal Processing for Communication Systems*, 2nd ed. New York: River Publishers, Sep. 2022.

[12] F. Marvasti, Ed., *Nonuniform Sampling: Theory and Practice*, ser. Information Technology: Transmission, Processing, and Storage. Boston, MA: Springer US, 2001.

[13] M. Grant and S. Boyd, "CVX: matlab software for disciplined convex programming, version 2.1," Mar. 2014.

[14] A. Dutt and V. Rokhlin, "Fast fourier transforms for nonequispaced data," *SIAM J. Sci. Comput.*, vol. 14, no. 6, pp. 1368–1393, Nov. 1993.